REVIEW ON THE MECHANICAL PROPERTIES, CRACK AND FATIGUE OF FRICTION STIR WELDS AND FLASH BUTT WELDS ON THE STRUCTURAL STEEL CONSTRUCTION

Fauzri FAHIMUDDIN
Doctor of Engineering, Civil Engineering Department, State Polytechnic of Jakarta, Indonesia, e-mail: fauzri.fahimuddin@sipil.pnj.ac.id

Taufiq ROCHMAN
Professor, Head of Structural Engineering Laboratory, Civil Engineering Department, State Polytechnic of Malang, Malang, Jawa Timur, Indonesia, e-mail: taufiq.rochman@polinema.ac.id

Abstract. This paper presents a comprehensive review of recent advancements in the mechanical properties, crack behavior, and fatigue performance of friction stir welds (FSWs) and flash butt welds (FBWs) on the structural steel construction. Friction stir welding (FSW) gained significant traction in various industries due to its capability to join different materials, including pure, alloy, and composite materials, and its application in aerospace, shipbuilding, railway, and automotive sectors. Despite its advantages, challenges such as high heat-induced weakening of residues and formation of defects in dissimilar material welds persist. This review also covers advancements in flash butt welding (FBW), particularly for rail joining, which includes analyses of temperature distribution, joint strength, and the impact of process parameters on weld quality. The paper further explores the heat-affected zone (HAZ) in both FSW and FBW processes, detailing the microstructural changes and their implications on weld performance and fatigue life. Key findings include the effects of temperature on HAZ microstructure and the development of novel methods for evaluating weld quality and fatigue resistance. This study aims to provide insights into ongoing research and potential improvements in welding technologies.

Key words: friction stir welding, flash butt welding, crack behavior, fatigue performance, structural steel construction.

1. Introduction

Among modern joining techniques, Friction Stir Welding (FSW) stood out as a versatile process that has revolutionized the field of materials joining. This solid-state welding method demonstrated exceptional capability in joining diverse materials, seamlessly connecting pure metals, alloys, and composite materials with high efficiency and reliability. Additionally, it was capable of welding dissimilar materials using the same method. In recent times, the FSW process had been employed to manufacture aerospace, shipbuilding, railway, and automotive components (El-Sayed *et al.*, 2021) and widely regarded as the most notable advancement in metal joining over the past twenty years (Singh *et al.*, 2018).

There was a significant lack of research in the investigation of tools that have multiple shoulders, which suggested a promising area for future (Khaliq *et al.*, 2023), also microstructural evaluation of welded joints (Królicka *et al.*, 2020) and the fatigue experiment and assessment of butt welded joint (Cui *et al.*, 2024).

However, the high levels of heat produced during friction stir welding (FSW) cause significant weakening and dissolution of the strengthening precipitated in AA6061-T6 butt welded joints. To address this challenge, a review study had been developed by Ogunsemi *et al.* (2021) that presented a range of improvement strategies from previous research that had been developed to enhance the overall performance in different processing conditions. Another researcher has reported successful utilization of the friction stir welding process to join dissimilar materials such as copper and aluminium. They stated that the primary categories of defects comprise tunneling, cavities, and voids, cracks, keyholes, and weld thinning. It was important to mention that the improper interaction between the base metals (BM) and the formation of intermetallic phases were the main factors that significantly contribute to the formation of defective welds (Isa *et al.*, 2021). Life Cycle Assessment (LCA) could be conducted for FST (friction stir techniques) to evaluate their environmental impact and identify potential strategies for mitigating these impacts (Prabhakar *et al.*, 2022).

The motivation for this review arose from the need to address critical gaps in understanding the mechanical properties, crack behavior, and fatigue performance of friction stir welds and flash butt welds in structural steel construction. The primary purpose of this paper was to synthesize and analyze existing research on these welding methods, focusing on their applicability and performance in structural applications. The objectives include evaluating the mechanical characteristics of these welds, understanding the mechanisms of crack initiation and propagation, and exploring factors affecting fatigue life. This review aims to provide a comprehensive perspective to support the optimization and broader adoption of these welding techniques in structural steel construction.

2. Welding techniques and defects

2.1 Flash Butt Welds and their defects

The forging stage of rail flash welding determined joint strength, and the process's temperature distribution improved the strength. The simulated rail end reached a peak temperature of 1906.9°C, significantly surpassing the melting point of the rail steel such depicted in Fig. 1 (Xu *et al.*, 2024).

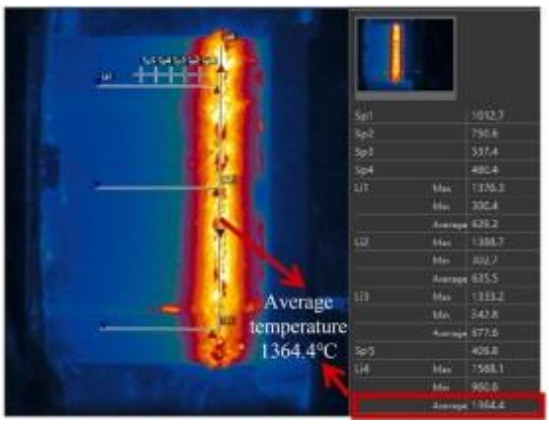

Fig. 1. Infrared temperature results, temperature measuring position (Xu *et al.*, 2024).

The Flash Butt Welding (FBW) process was preferred for rail joining due to its superior joint quality compared to thermite welding. Other study had been utilized a statistically designed experimental array to investigate four parameters of the FBW process, which the microhardness maps of the welded joints, under various welding conditions, for the Super Premium rail steels were displayed in Fig. 2 (Bauri *et al.*, 2020).

Based on the calibration results of the steel ruler and the actual image size, the length of the steel ruler was 10 centimeters. Three temperature lines were chosen consecutively on the rail head, rail web, and rail flange for the purpose of measurement and analysis, as depicted in Fig. 1 (Xu *et al.*, 2024).

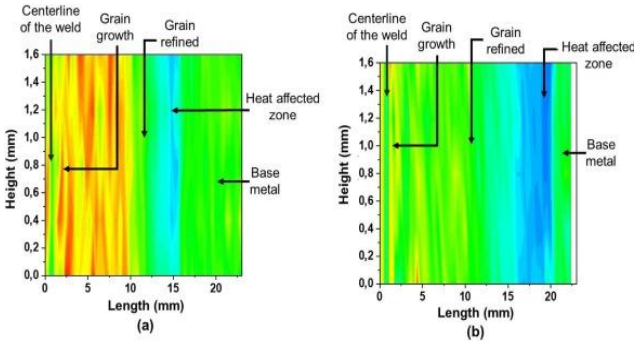

Fig. 2. Super Premium rail's Vickers microhardness (Xu *et al.*, 2024).

2.2 Cold Butt Welds and their defects

Cold Butt Welding (CBW) utilized plastic deformation to facilitate the production of joints at room temperature that possessed similar strength to their BMs. A beneficial technique that enabled the creation of strong connections without compromising the mechanical characteristics of the BMs stated by Celotto *et al.* (2024). The microstructure of the dissimilar joint between 1070 and 6082 highlighted a distinctive feature, as depicted in Fig. 3. A distinctive curved contact zone was observed, where the more rigid AA6082 wire penetrated the less rigid AA1070 wire, forming a U-shaped interface bond line. The white dashed lines represented the configuration of the joined interface, while the arrows indicated the direction of material movement during the process of upsetting (Celotto *et al.,* 2024). Their study addressed the research gap by investigating Cold Butt Welding (CBW) between two aluminium alloys with notably different mechanical properties: AA1070, with a yield strength of approximately 120 MPa, and AA6082, with a yield strength of 350 MPa. The base materials used were soft AA1070 and hard AA6082, both supplied as spools of Ø1.4 mm welding wires. An aluminum alloy named AA1070, with 99.7% Al, offers excellent corrosion resistance, high thermal and electrical conductivity (~62% IACS), and great formability but low strength, making it ideal for electrical conductors and decorative items. In contrast, AA6082, a 6xxx series alloy containing magnesium (0.6–1.2%), silicon (0.7–1.3%), and manganese (0.4–1.0%), provided medium to high strength, good corrosion resistance (including in marine environments), and excellent machinability. Its balance of strength and weldability made it suitable for structural, marine, and aerospace applications.

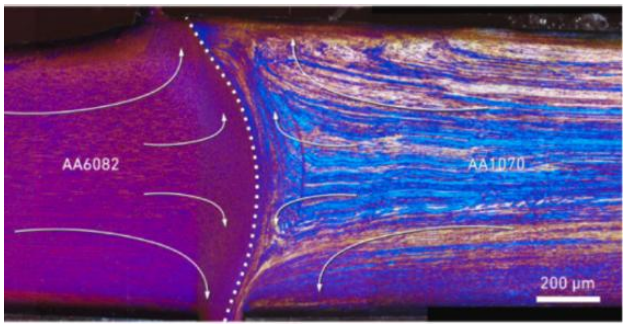

Fig. 3. A distinctive U-shaped contact zone of the dissimilar 1070–6082 joint in the white dashed line (Celotto *et al.,* 2024).

A novel method was suggested to measure the difference between electric-current and electrode-position signals obtained during the flash welding process using a spatiotemporal warping approach. Their experimental results have shown that the proposed methodology not only accurately identified the directional differences among flash welding profiles, but also surpasses traditional clustering algorithms by a significant margin (Chen *et al.,* 2019). Other study proposed the model that could be utilized to evaluate the fatigue life and design fatigue stress amplitude of steel rebars that were connected through flash butt welding. The model presented a potentially advantageous alternative to fatigue testing (Sheng *et al.,* 2024).

The study on the damage behaviour of rail flash-butt welding joints under controlled impact kinetic energy identified three key zones that revealing distinct damage mechanisms developed by Shen *et al.* (2024). By analyzing impact wear characteristics, their research offered a predictive framework for damage evolution, addressing critical weak points in railway track integrity. Their results highlighted significant variations in material properties, influencing the track's service life. Another study pointed out that the flash-butt welding process enhanced the strength and ductility of an IN718 alloy joint by optimizing the distribution of a diverse microstructure through controlled upsetting deformation (Zhou *et al.,* 2023). Other study examined the dimensions of the hot-rolled 440CL HSLA steel pairs used in the experiment were 70×10×6 mm. The steel composition consisted of 0.08% carbon (C), 1.188% manganese (Mn), 0.06% silicon (Si), 0.025% aluminum (Al), 0.017% chromium (Cr), 0.017% titanium (Ti), 0.014% phosphorus (P), 0.019% sulfur (S), 0.007% niobium (Nb), 0.005% nitrogen (N), and the remaining balance being iron (Fe), all in weight percentages. The welding process was performed using a Gleeble 3500 thermo-mechanical simulator (Wang *et al.,* 2021). Other study focused on analyzing the key process parameters involved in flash butt welding of mild steel brake tension rods. Specifically, the rate of current flow, heating time, flashing method, and initial distance between the jaws were examined to optimize the welding process (Rajesh and Devaraj, 2021). Several researchers examined flash welding such as FBW ductility of Inconel 718 joints (Zhou *et al.,* 2022), and numerical study on the ratcheting performance of FBW rails (Su *et al.,* 2021) and curved tracks (Wu *et al.,* 2022).

A comparative study had been conducted to analyze the changes in microstructure and mechanical properties of a Ti6242 alloy, which consists of both α and β phases, after undergoing FBW. Flawless bonding was achieved through the absence of welding defects while subjecting the material to a temperature gradient and deformation caused by upsetting (Xu *et al.,* 2020). Some researchers, such as Su *et al.* (2020) studied FBW ratcheting behavior under uniaxial and biaxial cyclic loadings, weldability of Inconel 718 using FBW (Zhu *et al.,* 2018), and FBW reliability analysis (Xu *et al.,* 2020), and using HSLA steel (Shajan *et al.,* 2019).

2.3. Linear Friction Welds (LFW)

Linear Friction Welding (LFW) was a solid-state welding technique that was widely used to join a wide range of products, ranging from small to large, made from similar or different materials. The study conducted by Mishra *et al.* (2023) employs linear friction welding to join two dissimilar materials. They conducted linear friction welding to examine the weldability of stainless steel with medium carbon steel. Another study explored by Miao *et al.* (2024) examined the factors that impact the fatigue life of LFW low carbon steel SM490A. The primary factors that were found to have the greatest impact on the LFW joints were the improvement of fatigue life and the mitigation of local stress concentration. Therefore, the act of joining with heightened force following the back-and-forth movement suggested in this research was a highly efficient approach to enhance the endurance of LFW joints. This was due to its ability to alter the contour of the weld edge depicted in Fig. 4 and diminish the concentration of stress (Miao *et al.*, 2024).

Other study suggested utilizing electric pulse treatment (EPT) to simultaneously enhance the TC17 LFW joint's strength and ductility by improving microstructure. Their study offered crucial insights into enhancing the strength and ductility of LFW TC17

titanium alloy blisked and expanding the use of LFW in aeroengine components (Zhang *et al.*, 2024). Other study performed by Yu *et al.* (2024) examined the impact of LFW on the microstructure, mechanical properties, and corrosion behavior of GH4169 superalloy.

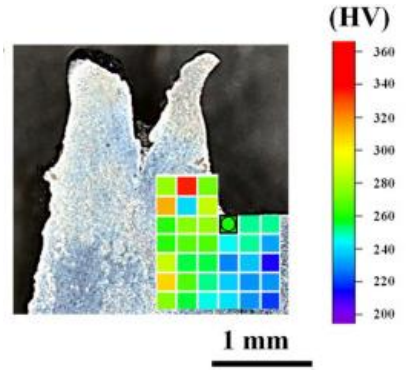

Fig. 4. Weld toe region's hardness distribution at the edge (Miao *et al.*, 2024).

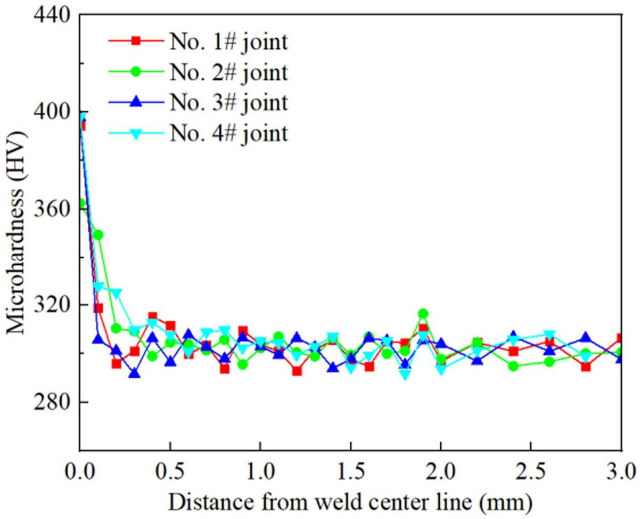

Fig. 5. Microhardness distribution of joints around weld center line, the highest hardness in No. 4# joint (Yu *et al.*, 2024).

The weld center zone exhibited higher hardness and tensile strength than the base material. They pointed out that as the grain size of the weld decreased, the fine-grain strengthening effect became more pronounced, resulting in increased strength and plasticity such depicted in Fig. 5. Corrosion resistance improved with increased joint shortening, though it decreased at higher solution temperatures. Notably, mechanical strength and corrosion resistance showed no significant correlation, allowing optimization of welding parameters to achieve high joint performance in both aspects (Yu *et al.*, 2024). Another study state that the microstructure of WZ (welded zone) exhibited a fine equiaxed crystal structure, while the TMAZ (thermos-mechanically affected zone) displayed a typical streamline structure. The BM structure consists of long strip structures aligned along the rolling direction. Fig. 6 shows the tensile specimen: (a) Macro morphology of joints (b) High multiple of area A (Xiao *et al.*, 2024).

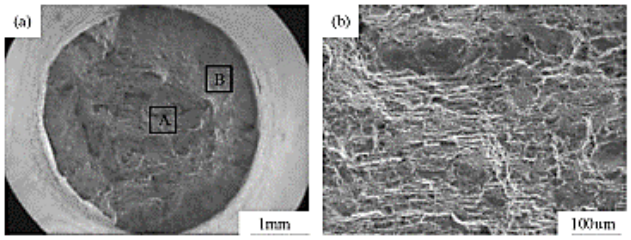

Fig. 6. Scanning electron microscopy (SEM) images illustrating the fracture morphology of tensile specimens (Xiao *et al.*, 2024).

Both numerical simulation and experimental research were conducted by Yu *et al.* (2024) to study LFW for GH4169 superalloy. The strain rate of the joint increased progressively as the welding frequency increased. Additionally, the thermoplastic metal experienced an increased in deformation resistance during the welding process, which prevented the timely extrusion of the thermoplastic metal at the interface, resulting in a decreased in joint shortening over time.

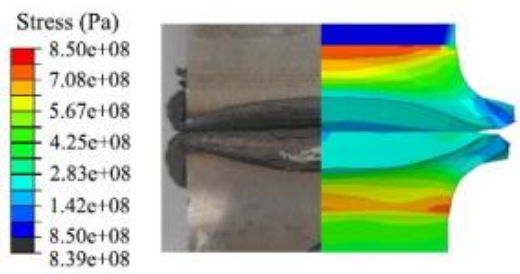

Fig. 7. Simulation vs experimental of macroscopic morphology (Yu *et al.*, 2024).

Fig. 7 compared simulation and experimental results of joint morphology, showing good agreement with evident curling. Then they highlights the shortening amount during welding, where the simulation shows 4.21 mm on one side, closely matching the experimental result of 4.15 mm under identical parameters (Yu *et al.*, 2024). A numerical correlation had been established by Peng *et al.* (2024) between the elastic constants and phase fraction of TC17 alloy to accurately determine residual stresses depicted Fig. 8 in linear friction welding.

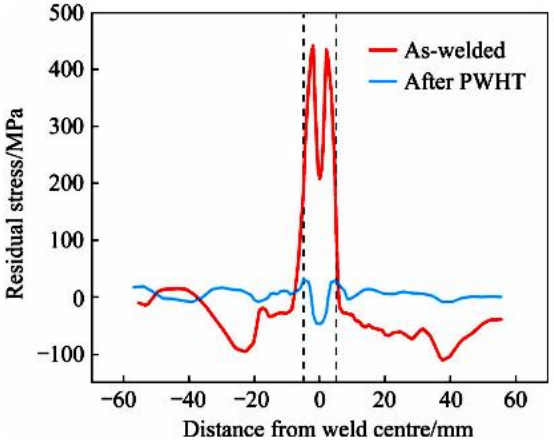

Fig. 8. The internal residual stresses on path of TC17 which was eliminated by PWHT become -47 MPa (Peng *et al.*, 2024).

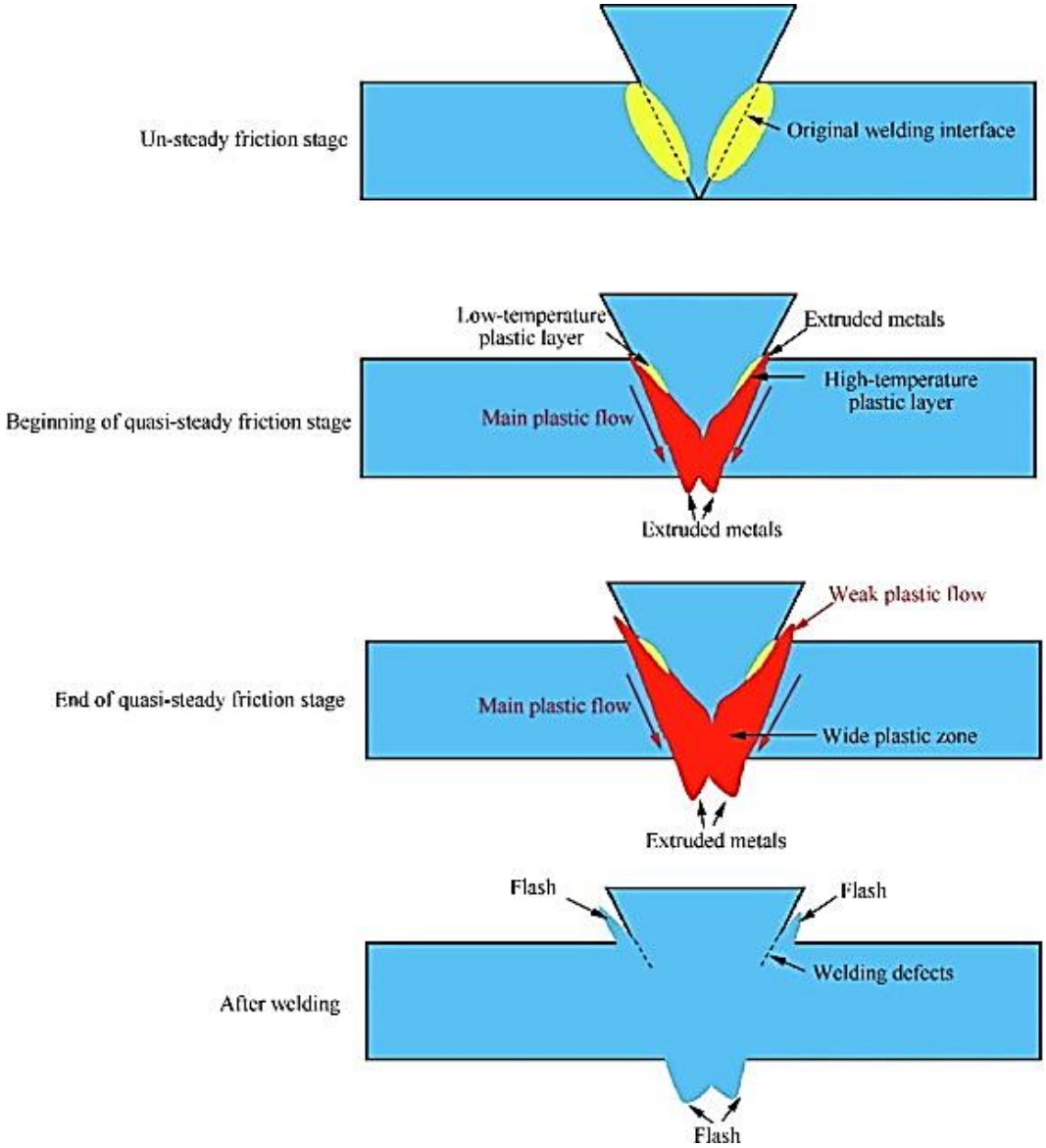

Fig. 9. Low temperature plastic layer, inverted V-shaped plastic flow during embedded LFW process (Tiejun *et al.*, 2024).

Several important results regarding LFW were found by Tiejun *et al.* (2024) that the plastic deformation in the oscillating direction was uniform. Thermo-plastic metals predominantly flew downwards along the welding interface in a perpendicular direction to the oscillation, leading to the formation of an inverted "V" shaped plastic zone such depicted in Fig. 9 at the interface.

The process of continuous dynamic recrystallization leads to the formation of interface bonding, which occurs simultaneously with significant dislocation motion and the generation of numerous low-angle grain boundaries (LAGBs). The grain orientation at the interfacial bonding area was characterized by randomness and a relatively low texture strength. The interfacial shear stress diminished during the process of continuous recrystallization (Tiejun *et al.*, 2024).

2.4. Friction Stir Welds (FSW)

Friction stir welding (FSW) in Fig. 10 was a contemporary welding technique that enabled the solid-state joining of two partners.

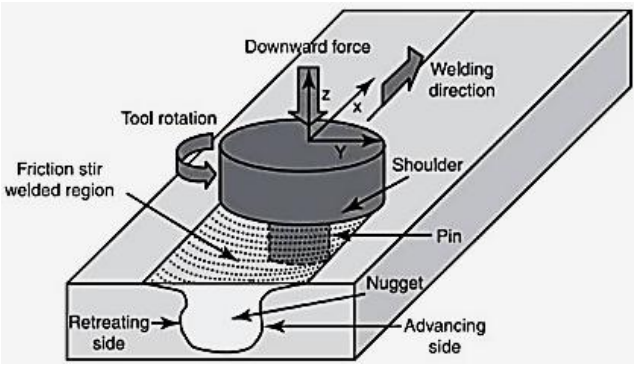

Fig. 10. A solid-state joining technique developed by The Welding Institute (TWI) called FSW that traversed along joint line (Singh *et al.*, 2018).

An inaccurate displacement weakened the connection, resulting in an unbalanced interpenetrating feature (IPF) and possible geometric flaws depicted in Fig. 11 (Khaliq *et al.*, 2023). The welding experiments were conducted using a Gebr. Heller Maschinenfabrik GmbH CNC milling machine model MCH 250, which was modified to carry out FSW.

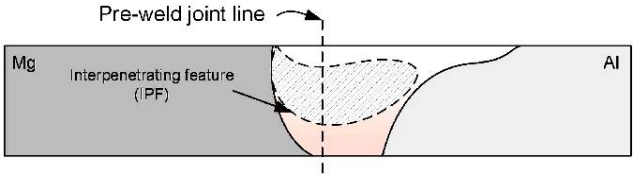

Fig. 11. Incorrect offset weakens the joint, leading to asymmetrical IPF due to tool offset and defects (Khaliq *et al.*, 2023).

They confirmed that presence of multiple alignment discrepancies depicted in Fig. 12 exacerbated the degradation of weld quality compared to single alignment discrepancies, because of the interactions between the factors (Vieltorf *et al.*, 2024).

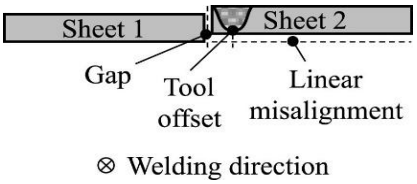

Fig. 12. Three alignment discrepancies (cross section) (Vieltorf *et al.*, 2024).

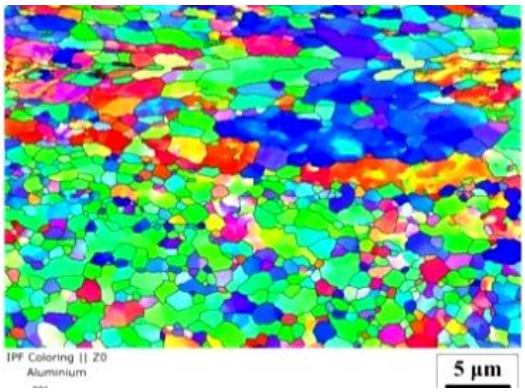

Fig. 13. ESBD analysis (Patel *et al.*, 2023).

The study had been conducted by Patel *et al.* (2023) examined the microstructures and mechanical properties of lap welds created using stationary shoulder friction stir welding (SSFSW). The SSFSW process achieved flawless welds with exceptional blending of materials in the SZ at welding speeds of 3 and 5 mm/s. The grain size in the SZ significantly decreased compared to both base materials,

indicating the remarkable dynamic recrystallization (DRX) in this region.

Fig. 13 presented the EBSD analysis results conducted on the SZ in the S4 weld, which revealed multiple features. The inverse pole figure (IPF) map in Fig. 18 illustrated a significant decreased in grain size in comparison to the base materials. It reveals two distinct types of grains: larger grains aligned along the (111) direction and smaller grains aligned along the (101) direction (Patel *et al.,* 2023).

The kissing bond defect typically arose at the weld root or at the interface between the base materials, as illustrated in Fig. 14a).The FSW tool did not penetrate the large distance at the bottom of the joined sheets, as shown in Fig. 14b). The occurrence of flash defect was caused by the excessive expulsion of plasticized material on the upper surface, resulting in a corrugated or ribbon-like appearance along the retreating side, as shown in Fig. 19c). A groove defect, as shown in Fig. 19d), was a pothole that develops on the surface of a welded joint because of an excessively small or large tilting angle, which may resulted in a limited amount of downward shaping of the plasticized material (El-Sayed *et al.*, 2021).

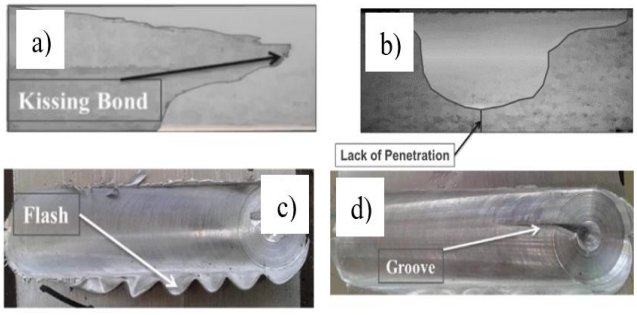

Fig. 14. Defects: kissing bond, lack of penetration, flash, and groove defects at the FSW interface of plasticized material (El-Sayed *et al.*, 2021).

The macro-section analysis and microhardness testing revealed that the reversed direct-squeeze friction stir welding (DS-FSW) technique exhibited superior mechanical properties in comparison to the conventional static shoulder friction stir welding (SS-FSW) method. Significant deterioration in the tensile properties such depicted in Fig. 15 was observed in the highly effective hybrid joint area of the AA2024-T3 to AA2198-T8 weld, which was produced using the reversed double-sided friction stir welding (DS-FSW) technique (Alemdar *et al.*, 2023).

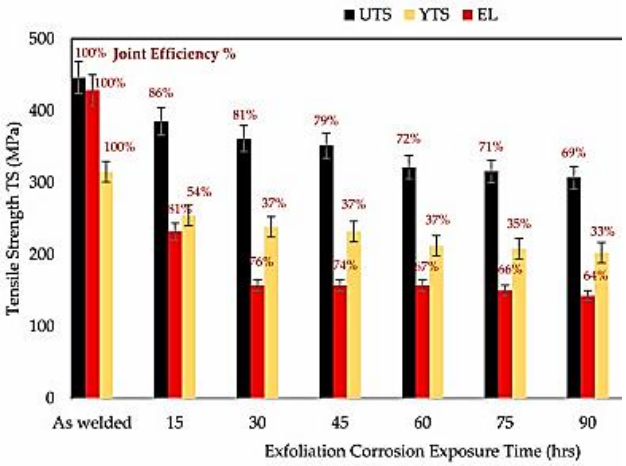

Fig. 15. Significant deterioration of tensile and elongation after the different durations of exposure to exfoliation corrosion using DS-FSW technique (Alemdar *et al.*, 2023).

A study has been presented on the analysis of the microstructure and mechanical properties of friction stir welded (FSW) joints, with a focus on the plastic flow and stirring of metal in the joint zone. Their analysis specifically examined thin sheets. They pointed out that the obtained joints have exhibited a durability ranging from 80-90% in comparison to the parent materials (Sliwa *et al.*, 2019). Another researcher found that during the process of welding, the welding force and temperature both escalated as the weld materials were rotated. The microstructure of the weld was influenced by an increased in the HAZ area, resulting in a softening of the weld's microstructure. The fracture strength measured 63.5 kN, while the weld strength was approximately 117 MPa, slightly below the BM's strength (Yasui *et al.*, 2018).

Another study had been conducted by Silva *et al.* (2023) conducted a numerical and experimental analysis of the factors that influence the friction stir welding (FSW) process using AISI 410S stainless steels. When the temperature in the stir zone approached 80% of the melting temperature, the likelihood of weld defects was greatly diminished. Colder temperatures could lead to issues with mixing, while hotter temperatures could resulted in the occurrence of flashes (Silva *et al.*, 2023). In test no. 4 (22 kN in Fig. 16c), the simulation observed a maximum temperature near the melting point. This proximity to the melting point could promote the formation of flash, as materials with lower viscosity would be expelled. As the temperature rose, the likelihood of welding defects also increased. Fig. 16d) and e) demonstrated the expansion of the high-temperature area (Silva *et al.*, 2023).

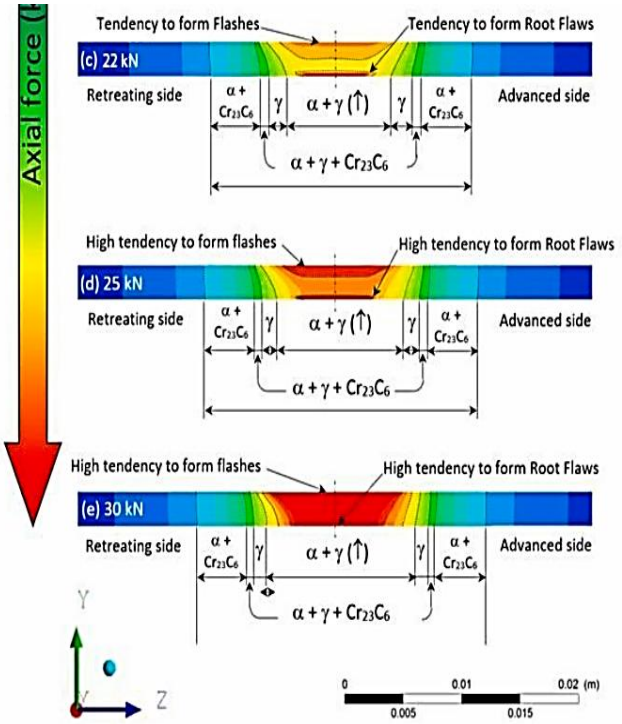

Fig. 16. Temperature cross-section with a rotation of 800 rpm at: c) 22 kN; d) 25 kN ; and e) 30 kN at 80% melting temperature using AISI 410S stainless steels (Silva *et al.*, 2023).

Ultralight Mg–14Li–1Al alloy sheets were used in a comparative study to investigate the effects of conventional FSW and rapid cooling FSW (RCFSW). Utilizing coolant had a more pronounced effect on enhancing the thermal cycle and preventing grain coarsening compared to reducing the rotation rate.

The UTS (ultimate tensile strength) and fracture elongation of the conventional FSW LA141 joint could be increased to 182 MPa and 8.3%, respectively, by decreasing the rotation rate. In contrast, the UTS and elongation of the RCFSW600 joint were measured to be 181 MPa and 9.6%, respectively (Xu *et al.*, 2023).

3. HAZ, Other Defects and Mechanical Properties

3.1. Heat affected zone (HAZ)

The heat affected zone (HAZ) refers to the area that underwent a thermal cycle without any plastic deformation. Consequently, the heat generated did not affect the evolution of the microstructure. Nevertheless, El-Sayed *et al.* (2021) said that when the temperature of a heat-treatable aluminum alloy exceeds 250°C, it has a notable effect on the structure of the precipitation, causing them to coarsen. A novel twin-disc experiment was conducted utilizing discs that encompassed all microstructures found in the HAZ of flash-butt welded rails. They said that extended crack lengths or clusters of cracks were detected in the HAZ boundary and the central weld regions (Shen *et al.*, 2024).

The results had been summarized by Bai *et al.* (2023) indicated that the HAZ subzones displayed intricate microstructures that vary depending on the peak temperatures (PTs). As the PT increased, the prevailing microstructure type in the HAZ evolved from polygonal bainitic ferrite at 700 °C to a combination of fine bainitic ferrite and granular bainite at temperatures ranging from 850 to 1000 °C, and ultimately to coarse bainitic ferrite and granular bainite at

1350 °C. Impact tests revealed that the impact toughness shows a notable increased as the PT reached 920 °C specifically, in the fine-grained heat affected zone (FGHAZ). However, beyond this temperature, the impact toughness began to decline. The FGHAZ exhibited the highest impact toughness among HAZs, although it was still lower than that of the BM. During the welding process, the microstructure of the joint will undergo changes compared to the original microstructure. This was caused by the formation of a HAZ, which could negatively impact the mechanical properties of the joint. Their materials used was high-strength carbide-free bainitic (CFB) rail steel. Welding thermal simulations were conducted using a Gleeble-3500 simulator to replicate peak temperatures (PT) for each heat-affected zone (HAZ) subzone. The resulting microstructures were analysed, and impact toughness was evaluated using instrumented Charpy impact tests. The research revealed distinct correlations between welding PT and microstructural evolution, with differences in fracture morphologies and crack propagation modes across HAZ subzones (Bai *et al.*, 2023).

Continuing the previous research have developed by Shen *et al.* (2024), they stated that the extended crack lengths or clusters of cracks were observed in the HAZ boundary and central weld regions. They added that the cross-sectional metallography analysis revealed that these cracks were specifically associated with the microstructure of spheroidized cementite at the HAZ edges or pro-eutectoid ferrite at the central region (Pereira *et al.*, 2024). An experimental simulation was conducted to create a controlled aging process to study the microstructural gradient of the HAZ in aluminum alloy FSW. Their simulation aimed to assess the impact of the HAZ microstructural gradient on the rate of fatigue crack propagation, while disregarding the influence of weld residual stresses (Kermanidis and Tzamtzis, 2017).

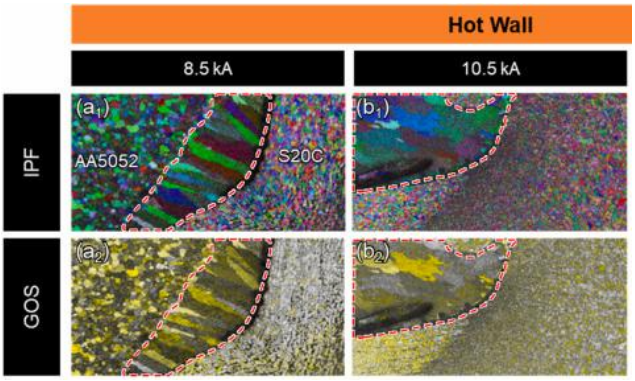

Fig. 17. EBSD results of the Al HAZ depending on welding hot and cold parameter (Baek *et al.*, 2024).

When considering hot wall joints, a dendrite-like Al HAZ was consistently detected under all welding current conditions. There was a significant difference in hardness between the Al HAZ in the hot wall case and the Al in the cold wall case without a HAZ such depicted in Fig. 17. The inclusion of Al HAZ had a significant influence on the hardness properties of the molten steel section. When using a welding current of 10.5 kA, the hot wall showed a roughly 30% higher tensile shear load and a 66% greater displacement compared to the cold wall configuration without HAZ (Baek *et al.*, 2024).

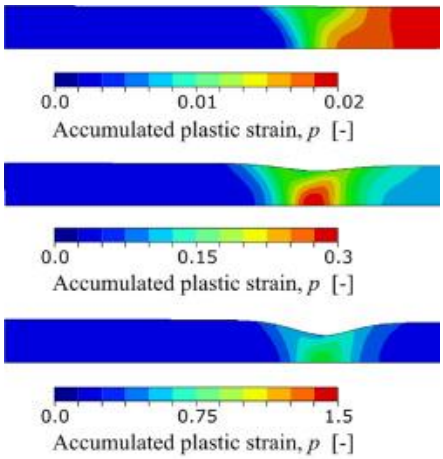

Fig. 18. The accumulated 2D plastic plane-strains contour within HAZ materials with CL model an quasi static conditions at: a) yielding; b) strain localization; and c) fracture (Aune *et al.*, 2024).

Subsequently, the fusion zone underwent a rapid increased in hardness due to work hardening, causing the plastic strains to concentrate within the HAZ materials until they eventually fractured (Aune *et al.*, 2024). The 2D plane-strain model deformation sequence with CL model and quasi-static conditions shown in Fig. 18.

A study has been conducted by Yan *et al.* (2023) examined the mechanical properties of the HAZ using a semi-empirical approach. They examined the mechanical properties of the HAZ using a semi-empirical approach. The HAZ of S355 and S500 exhibited an average reduction of 13% and 4% in yield and ultimate strength, compared to the BM depicted in Fig 19. The modification factors (MF1 and MF2) considered the transverse restriction caused by the BM and the weld metal (WM) on the HAZ, as this restriction enhanced the resistance of the HAZ (Yan *et al.*, 2024).

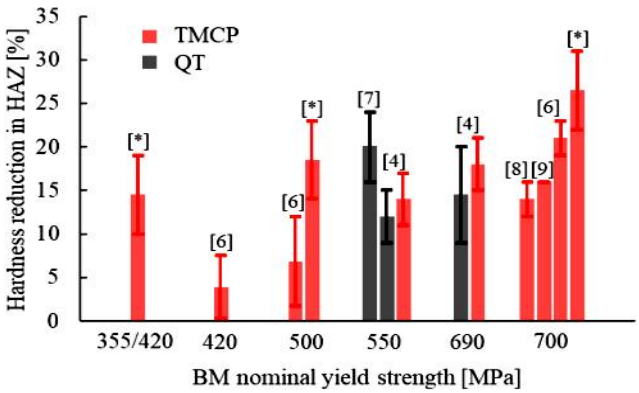

Fig. 19. Hardness reduction in HAZ vs. BM nominal yield strength (Yan *et al.*, 2024).

If the HAZ was the weakest part of a welded joint, both the WM and/or the BM will exert a transverse constraint on it, regardless of the steel grade. The greater the disparity in material hardening behavior between the HAZ and the WM and/or BM, the more pronounced the transverse constraint.

The use of digital image correlation (DIC) resulted such in Fig. 20 in an increased overestimation of the strength of the HAZ material (Yan *et al.*, 2022). A comprehensive analysis had been conducted by Maia *et al.* (2023) on the HAZ of 3 welded joints with varying heat-input conditions to assess the impact of reheating cycles and welding parameters on the microconstituents. They said that SCR-CGHAZ consistently demonstrated the highest microhardness values among all welding conditions. This aligns with the analysis of the cap passes, which indicated that the FGHAZ was the hardest region in the heat-affected zone. On the other hand, the SC-CGHAZ and IC-CGHAZ displayed lower microhardness values. Fig. 21 displayed microhardness maps of the fill passes HAZ in each sample, indicating heterogeneous HAZ with distinct regions based on microhardness values.

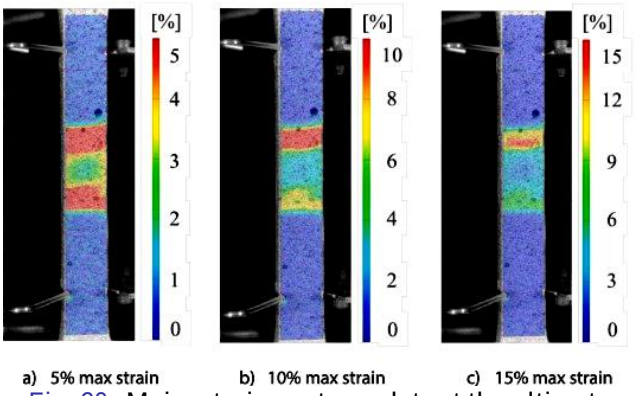

Fig. 20. Major strain contour plots at the ultimate load (Yan *et al.*, 2022).

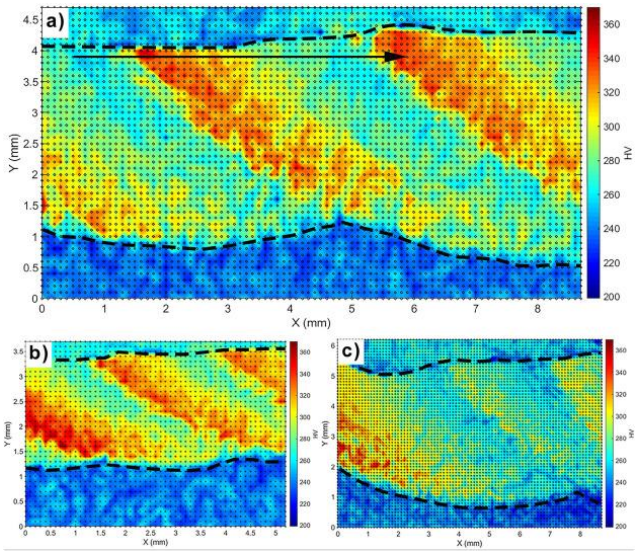

Fig. 21. Microhardness mapping over reheated HAZ of fill passed on samples of a) medium heat-input; b) low and; c) high heat-input (Maia *et al.*, 2023).

In Fig. 21 a-c, the upper area of light blue tones was the FZ, while the lower area of dark blue tones (lower microhardness) was the BM (Maia *et al.*, 2023).

3.2. Defect types, location, and aspect ratio

To ensure the rational performance of a welded structural member, the potential presence of welding defects must be carefully considered regarding its fitness for purpose. Consequently, it was essential to assess the fatigue performance of welded joints that contain various defects.

A study had been conducted on the fatigue performance of butt-welded joint specimens with five distinct types of defects, differing in size and location, across a broad range of fatigue life. The defect usually contained in specimens were crack (CR), incomplete penetration (IP), lack of fusion (LOF), slag-inclusion (SI), and blowhole (BH), which were vary in size and location. The CR type defect usually was weld-hot crack such depicted in Fig. 22.

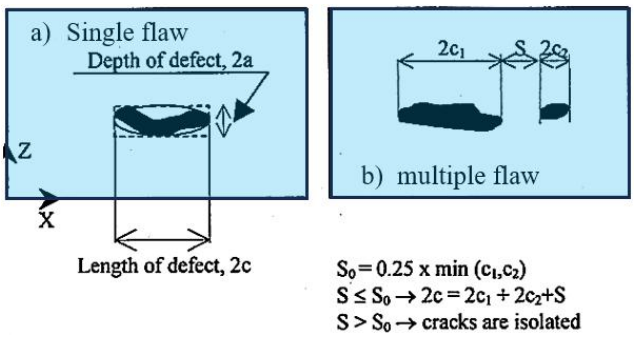

Fig. 22. Illustration of defects and their length (Miki *et al.*, 2001).

This kind of crack type defect often occurs in the first layer of multipass welding, therefore CR type of this defect installed on the first layer in their study. The depth of defect was almost impossible detected by RT (radiographic testing).

In order to evaluate the RT results, the detected defect's length on failure surfaces were measured after the fatigue test. These measured results called as real size was compared with the RT results as shown in Fig. 23 (Miki *et al.*, 2001).

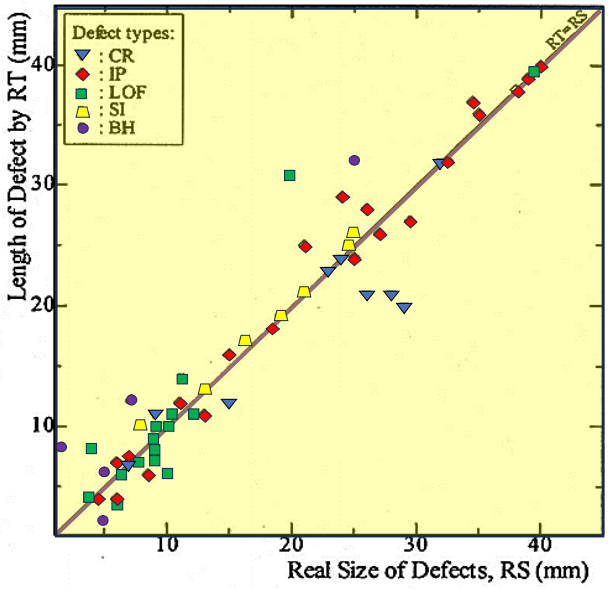

Fig. 23. Comparison between RT and real size defects such cracks, incomplete penetration, lack of fusion, slag-inclusion and blowhole (Miki *et al.*, 2001).

3.3. Fatigue Performance

The study had been developed by Zhao *et al.* (2015) examined the fatigue fracture mechanism of flash butt welding joints of U75V rail steel by analyzing their microstructure, hardness, S–N curve, and fatigue fracture resulting from two different welding procedures. They found that the fatigue performance of flash welding joints was primarily determined by the level of upset pressure such depicted in Fig. 24.

Increasing the pressure above the normal level was beneficial for enhancing the resistance to fatigue. The fatigue crack originated from the interface area and subsurface of the sample in the presence of a corrosive environment (Zhao *et al.*, 2015). An investigation had been conducted to analyze the tensile strength, fatigue strength, fatigue surface characteristics, and fatigue crack propagation of the hybrid shoulder friction stir welded (HS-FSW) joint in an Al-Mg-Si alloy depicted in Fig. 25. They concluded that HS-FSW joint exhibited exceptional fatigue characteristics (Zhang *et*

al., 2023). When the IMCs layer was thin, the Al/steel interface would form a strong metallurgical bond, resulting in increased strength and fatigue resistance of the joints. However, if the IMCs layer at the interface became excessively thick, it could cause cracks and could decrease the load-bearing capacity of the joint (Liu *et al.*, 2023).

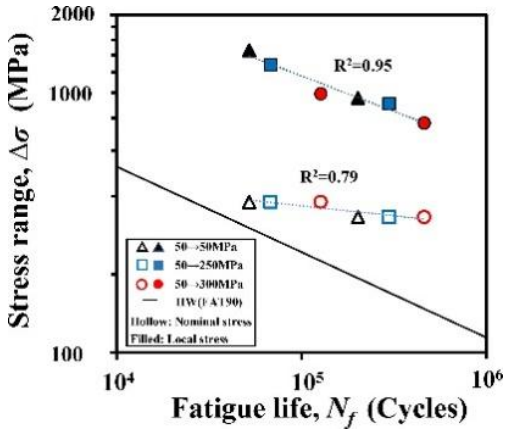

a)

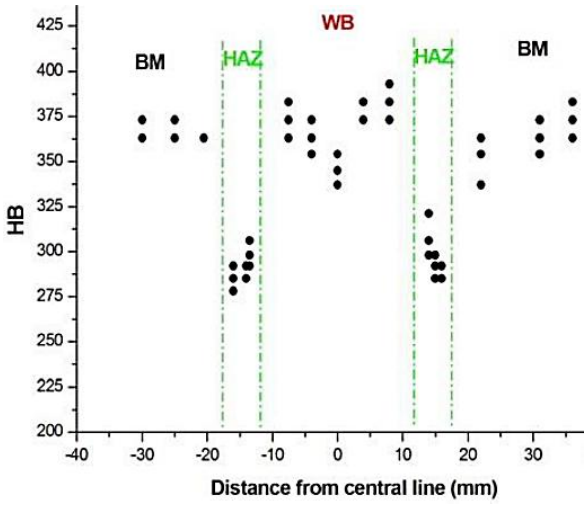

b)

Fig. 24. a) Local stress range vs fatigue life cycles (Miao *et al.*, 2024); b) Brinell Hardness (HB) data, BM=base metal, WB=weld bead, HAZ=heat affected zone (Godefroid *et al.*, 2014).

Another study determined that fatigue cracks originated near the weld bead depicted in Fig. 26 and propagated in a brittle manner, resulting in premature material failure (Godefroid *et al.*, 2014). An experimental study has been performed by Sheng *et al.* (2020) was conducted to investigate the tensile and high-cycle fatigue properties of HRB500 high-strength steel rebars that were joined using flash butt welding. The fatigue strengths of welded specimens decreased as their diameters increase, and the reduction in high-cycle fatigue strength was more pronounced for large-diameter welded specimens. Welded specimens of HRB500 high-strength steel rebars were more susceptible to premature fatigue failure compared to the base materials. Additionally, the rate at which the fatigue strength of welded specimens decreased with increasing loading cycles diminished (Sheng *et al.*, 2020).

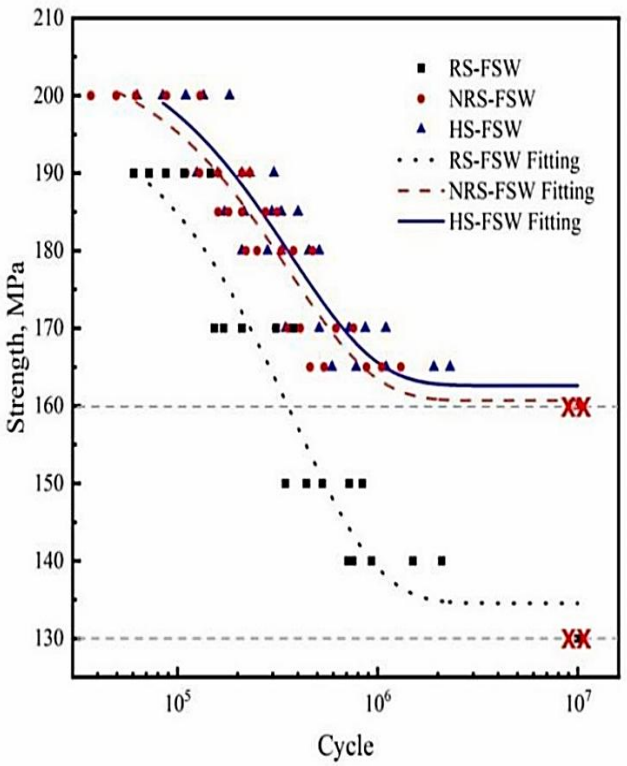

Fig. 25. The fatigue test results of the RS-FSW, NRS-FSW and HS-FSW joints (the highest) in Al-Mg-Si alloy (Zhang *et al.*, 2023).

A coupled finite element method (FEM) that incorporated thermal, metallurgical, and mechanical factors was utilized by Ghazanfari and Tehrani (2021) to assess the fatigue life and determine the angle at which cracks initiate in welded rails. Their analysis was based on the critical plane method. FBW optimization was conducted to enhance fatigue life (Ghazanfari and Tehrani, 2021).

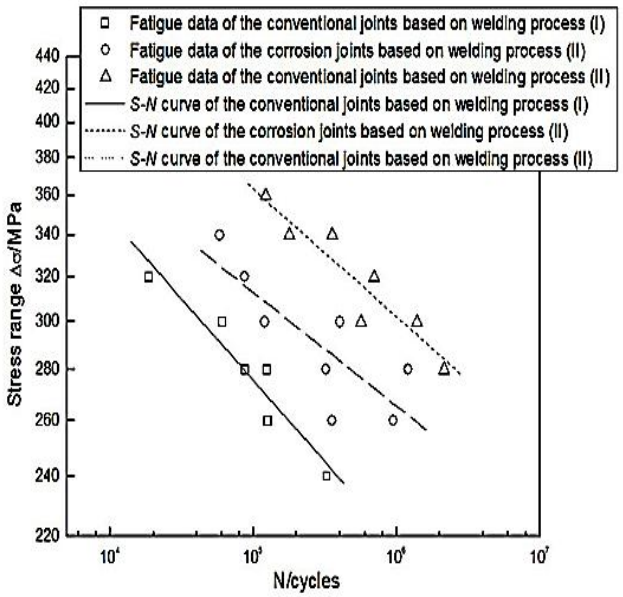

Fig. 26. Stress-N cycles curve of conventional and corrosion joints under three welding processes condition (Zhao *et al.,* 2015).

The S-N curves for fatigue demonstrated that the fatigue life of the specimens was enhanced by Li *et al.* (2022) using LSP (laser shock peening) treatment, especially when subjected to low levels of bending stress. The fatigue limit experienced a 6.7% increase, rising from 264.0 MPa. The fatigue fracture analysis showed that the presence of high-density dislocations increased the resistance to the growth of fatigue cracks. As a result, the area where the crack propagated near the surface treated with LSP exhibited a rough morphology characterized by steps (Li *et al.*, 2022). The fusion line in the flash butt weld exhibited lower toughness when compared to the CGHAZ, FGHAZ, and parent material (Shajan *et al.*, 2019).

The test results had been utilized by Trimech *et al.* (2023) to examine the fatigue failure mode of this distinct joint type and to establish the S-N curve that was valuable for characterizing and designing fatigue-sensitive components. The fatigue data was evaluated utilizing the effective notch stress (ENS) methodology, as advised by the International Institute of Welding (IIW). The results indicated that the IIW design ENS IIW FAT-71 curve, which was based on fatigue tests conducted on fusion-welded joints, was overly cautious when evaluating the fatigue performance of butt-lap friction stir welded (FSW) joints, particularly in the high cycle range (Trimech *et al.*, 2023).

When the stress range was 380 MPa, the fatigue life of the LFW as-welded joints increased by around 31% when the pressure after oscillation was 250 MPa, compared to a pressure of 50 MPa. Similarly, when the pressure after oscillation was 300 MPa, the fatigue life increased by 87% compared to a pressure of 250 MPa. Although there was a chance of fractures starting at the weld toe on the edge of the LFW joints, the fatigue strength showed a significantly longer fatigue life compared to the S-N design curve FAT90 recommended by the IIW (Miao *et al.*, 2023).

A thorough investigation has been done by Liu *et al.* (2023) conducted to analyze and describe the fatigue fracture properties of linear friction welded Ti17 joint and Ti17 joint after undergoing different post welding heat treatment (PWHT) methods. Their results indicated that the Ti17 joint, as welded, tends to fracture at the weld centerline zone (WCZ) and the TMAZ during fatigue service. The joint has a fatigue life of 45201. The fracture occurs in a heterogeneous structure consisting of refined equiaxed β grain, coarse β grain, and basket-weave β grain with partially dissolved lamellar α. This structure corresponded to the weld centerline zone (WCZ), the TMAZ, the HAZ, and the BM (Liu *et al.*, 2023).

The results had been done by Miki *et al.* (2001) reveal that the shape, size, and location of these defects significantly influence the fatigue performance of the specimens. Fatigue test results were plotted

in S-N curve depicted Fig. 27 represented the specimen that contain CR type defects.

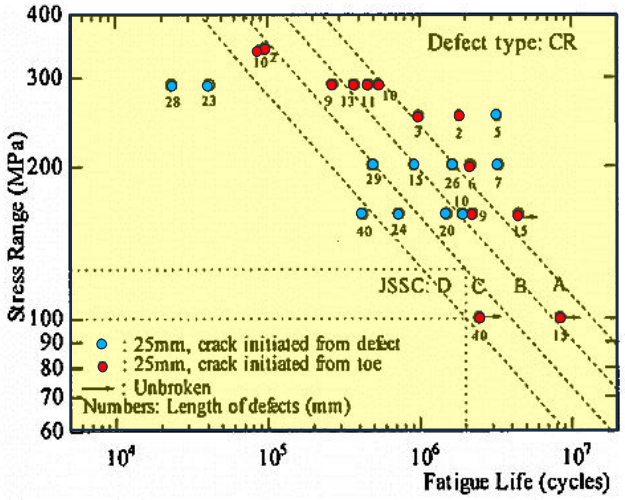

Fig. 27. Fatigue test results: S-N curve for CR type defect (Miki *et al.*, 2001).

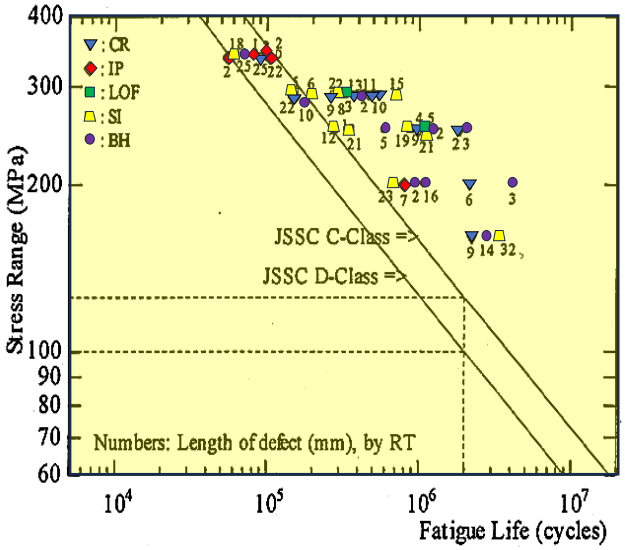

Fig. 28. Stress-N cycles summary of observed failure specimens with fatigue crack originated from weld toe (Miki *et al.*, 2001).

Some of specimen failed with fatigue cracks originated from the embedded defects, and some other specimen have fatigue cracks initiated from weld-toes. The cracks from defects were indicated by blue circle in the S-N curves, while cracks from weld-toes were indicated by red circles. The number beside the symbols indicated the defect's size in length 2c, as illustrated in Fig 22. A number of specimens were observed to failure with fatigue cracks originated from weld toe as summarized in Fig. 28.

By using fracture mechanics analysis, critical defect size could be calculated which was shown in Fig. 29. By applying 100 MPa stress range for the fatigue life of 2.10^6 cycles, the critical defect size of about 4.2-mm was obtained. The result was smaller compared to the experimental result, which was reasonable, because the initiation fatigue life was not take into account in the analysis. However, the value was conservative, therefore further study was necessary in order to get more suitable results from fracture mechanics analysis. For joint with larger plate thickness that have similar geometry as the 25-mm joint specimen the permissible defect sizes were little bit larger as shown in Fig. 22.

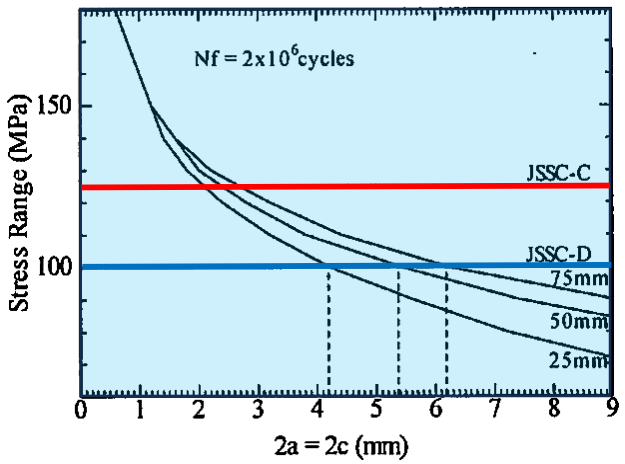

Fig. 29. Critical and permissible defect size based on 100 MPa stress range and 2.10^6 cycles fracture mechanics analysis (Miki *et al.*, 2001).

Therefore, in the case of the change of plate thickness to the thicker one there was a possibility the same value of 10-mm could be applied. Fatigue life predictions, based on fracture mechanics analysis following this recommendations, tend to be conservative in the long-life region (Miki *et al.*, 2001).

3.4. Fracture or cracks

An investigation has been conducted by Xu *et al.* (2016) to analyze the failure modes and fracture mechanism of the wheel rim that have failed. Their study assessed the

microstructure and fracture mechanism of a flash butt welded 380CL steel by comparing the failed wheel rim with the intact wheel rim. The wheel rim's high yield ratio led to a lack of formability during the flaring process. The fracture mechanism of the rim that failed involved a combination of ductile and brittle fracture modes (Xu *et al.,* 2016).
The fracture surface of the U71Mn rail exhibited a prominent corrosion area, suggesting prolonged usage of the rail. The rail welding joint exhibited fatigue fracture as its characteristic feature such depicted in Fig. 30. During the process of straightening, transporting, laying, and serving, cracks propagate due to bending stress until they caused fracture (Yu *et al.,* 2015).

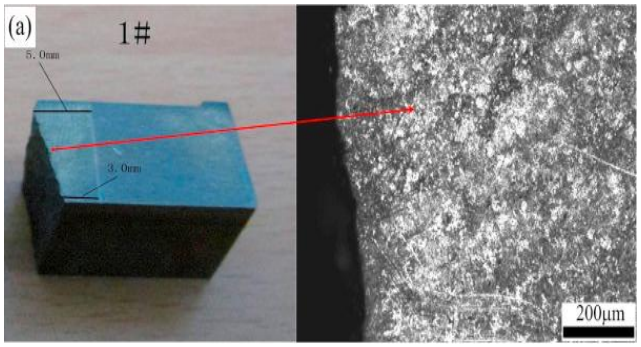

Fig. 30. Metallographic morphology of the rail welding joint and fracture surface edge (Yu *et al.,* 2015).

In the study had been developed by Hu *et al.* (2023), they used various macro and micro characterization tools to investigate the factors leading to the formation of surface cracks in a flash butt welding joint of a high manganese steel frog. Their findings indicated that these cracks were intergranular stress corrosion cracks (IGSCC) that were primarily located near the fusion line between the carbon steel rail and the stainless-steel medium on the stainless-steel side (Hu *et al.,* 2023).

When the value of Φ was 0, the elliptical pore had the most significant impact on the deformation of the creep crack at the prefabricated crack. Additionally, the crack propagation rate was the highest in this case. In general, the influence of pores on the propagation of creep cracks was more pronounced compared to that of inclusions such depicted in Fig. 31 (Yang *et al.,* 2024). Other study had been done by Owsinski *et al.* (2021) investigated the fracture behavior in welded steel. Cracks were observed to form in the parent material but away from the transformed weld region, revealing a potential connection to the heat-affected zone.

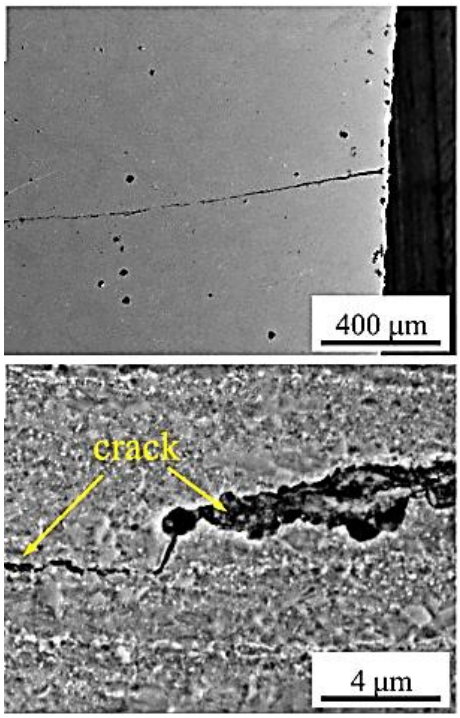

Fig. 31. SEM: a) overall morphology and cracks; (Yang *et al.,* 2024).

The orientation of crack planes relative to the nominal weld interface correlated with fracture patterns. By analyzing fracture points and interpolating a crack initiation plane, they suggested that residual stresses and angular orientation influence fracture direction and behavior in welded joints (Owsinski *et al.,* 2021).

A comprehensive FEM-based methodology was introduced to simulate the fatigue propagation of multiple cracks in friction stir weldments under cyclic tensile loading. The study incorporated both linear and non-

linear models, utilizing residual stresses from thermo-mechanical simulations. Vasudevan's, Kujawski–Ellyin, and UniGrow laws were employed to assess fatigue crack growth. Experimental defects were integrated using constrained crack faces technique, enabling accurate predictions of crack behavior under varying material condition (Lepore and Berto, 2019). The fatigue crack growth rate of the welded joint depicted in Fig. 32 was significantly affected by the relative rotational speed. Unequal rotational speeds between the tools cause an irregular stirring of the material, leading to flaws and a higher rate of fatigue crack growth with an *n* value of 4.307. On the other hand, maintaining a consistent rotational speed resulted in uniform material stirring, which leads to a decreased in defects and a reduction in the rate at which fatigue cracks spread, reaching an *n* value of 4.157 (Puspitasari, 2024).

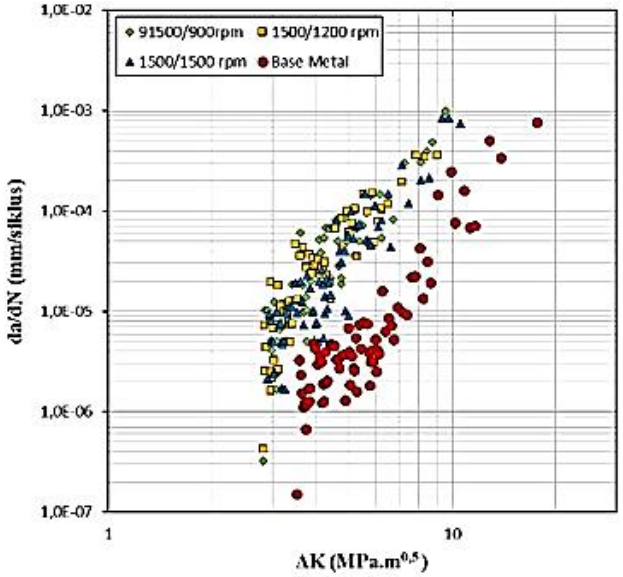

Fig. 32. Stress intensity factor versus fatigue crack growth rate (Puspitasari, 2024).

3.5. Mechanical Properties

Study had been conducted by Xi *et al.* (2016) investigated the microstructures and mechanical properties of flash butt welded high-strength RS590CL steel joints, revealing that weld thermal cycles were marked by high peak temperatures and rapid heating and cooling rates. The joint's microstructure included various zones with differing hardness and toughness. Excessive flash allowance significantly reduces joint toughness due to coarsened upper bainite, retained oxides, and defects in the weld interface zone. Optimizing flash allowance, upset allowance, and upset pressure enhanced joint toughness, matching base metal strength (Xi *et al.,* 2016). Also, the effect of tool rotational speed on the microstructure and mechanical properties of Al–Li alloy AA2198 during bobbin tool friction stir welding was investigated by Wang *et al.* (2015). As rotational speed increased, grain size in the stirred zone grows, and joint line remnants compress significantly in the shoulder-dominated zone. The hardness profile evolved from U-shaped to W-shaped, with joint efficiency peaking at 80%. Three fracture modes were identified, with cracking initiating at the joint line remnant. Their study highlights how rotational speed influenced joint strength, hardness distribution, and fracture behavior in Al–Li alloy welding (Wang *et al.,* 2015). The microstructural and mechanical properties of ductile cast iron and alloy steel joints, welded using magnetically impelled arc butt (MIAB) welding, were evaluated by Peng *et al.* (2021). Their study revealed that non-uniform heating during welding led to varying metal extrusion and changes in microstructure across the weld zones. A significant increased in weld hardness (482 HV) and tensile strength (382.4 MPa) was observed, highlighting the effectiveness of MIAB welding in joining these dissimilar materials, with tensile strength reaching up to 95.6% of the base metal such depicted in Fig. 33 (Peng *et al.,* 2021).

The study had been conducted by Pang *et al.* (2022) investigated the microstructures, mechanical properties, and residual stresses in PG4 flash-butt welded rail joints. Significant findings include a reduction in hardness within the heat-affected zone

(HAZ) and high heterogeneous strains, with grain misorientation affecting the weld's integrity. A key relationship between bond strength and HAZ width was established, revealing that strength was highest at the rail's foot and head but decreased at the web. High residual stresses were also identified, underscoring the importance of HAZ width in assessing weld quality and improving rail safety (Pang *et al.,* 2022).

The study had been developed by Li *et al.* (2020) presented an in-depth analysis of flash-butt welded TA19 joints, revealing that post-weld heat treatment (PWHT) significantly enhanced both ductility and strength.

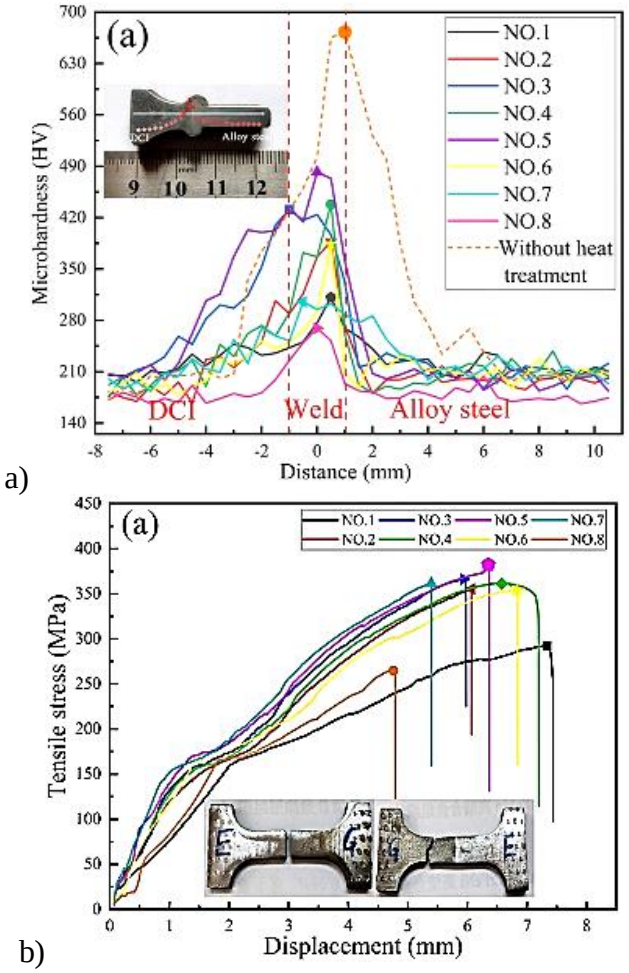

Fig. 33. a) Microhardness of MIAB welding joint; b) Tensile results (Peng *et al.,* 2021).

The uniform microstructure achieved through PWHT, including the relief of tensile residual stress and the formation of large α grains, contributed to a ~25% increased in ductility. Additionally, age hardening accounts for a ~90% increased in strength. Their research offered valuable insights into optimizing microstructural architecture to maintain high performance in welded titanium alloys (Li *et al.,* 2020). The study had been performed by Shen *et al.* (2018) examined the microstructure evolution and mechanical properties of flash butt-welded Inconel718 joints, highlighting the formation of a gradient structure in the heat-affected zone (HAZ) due to thermal and strain gradients. Grain growth and phase dissolution in the welding seam reduce ductility and strength, while coarsened grain boundary carbides lower impact toughness. Despite these challenges, the joints exhibited sufficient formability, offering valuable insights for improving the welding of Inconel718 and similar superalloys (Shen *et al.,* 2018).

The study had been conducted by Porcaro *et al.* (2019) investigated the microstructural evolution and mechanical properties of flash butt welded pearlitic steel rails, with a focus on the heat-affected zone (HAZ). Dilatometry revealed that larger austenitic grain size leads to austenite-pearlite transformation at lower temperatures, resulting in increased hardness in the grain growth region. Partial cementite spheroidization in the HAZ caused a decreased in hardness and tensile strength, linked to failures. Their study proposed a dilatometry-based methodology to optimize post-weld cooling, enhancing weld performance by improving hardness profiles without added costs or time (Porcaro *et al.,* 2019).

The study had been done by Yang *et al.* (2023) explored the microstructural evolution and mechanical properties of GH4169 superalloy joints produced via linear friction welding (LFW). Their results

showed that the weld zone exhibited a "W" shaped hardness profile, with microhardness varying across different zones. Material defects, such as pores and inclusions, were characterized, revealing that they impact joint performance. Tensile tests indicated that defects enriched with oxygen, oxides, and carbide particles initiate crack formation, leading to joint failure.

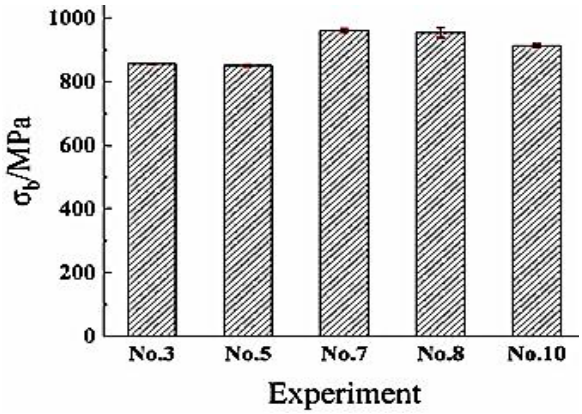

Fig. 34. Tensile strength (MPa) in GH4269 joints under different parameters via LFW process (Yang *et al.,* 2023).

Their findings highlighted the influence of welding variables on joint quality and provide insights for optimizing LFW of GH4169 superalloy. Their results were shown in Fig. 34 (Yang *et al.,* 2023).

4. Interpretation from Authors Perspective

The discussion of fatigue behavior in joints with defects has primarily focused on the length of the defects and the nominal stresses applied. However, the depth of the defects varied significantly, as well as their locations and the corresponding stress distribution, as highlighted earlier. These factors were critical for evaluating the fatigue behavior of joints containing defects. In this evaluation, only specimens that failed due to fatigue cracks initiated from embedded defects were considered. The fatigue behavior in the presence of defects depended on Eq. (1), the stress intensity factor associated with the initial crack shape.

$$K_0 = \sigma\sqrt{\pi \cdot a} \cdot F \quad (1)$$

$$F = F_g \cdot F_e \cdot F_t \cdot F_h \quad (2)$$

The parameter aa represented the half-depth of the defect, modeled based on a simplified crack. The correction factor F in Eq. (2) incorporated several influences, including the effects of the stress gradient (F_g), crack shape (F_e), plate thickness and width (F_t), and the eccentricity of the defect relative to the central axis of the plate (F_h).

The stress gradient was derived from the stress distribution in the X-direction, perpendicular to the defect plane, as determined through FEM analysis. The relationship between the initial stress intensity factor (K_0) and fatigue life (N_f) was represented by a regression line fitted to a power function. Results indicated that joint specimens with fatigue cracks initiated from embedded defects exhibited similar fatigue behaviour, regardless of the defect type. Fatigue life was influenced by the shape and location of the defect, which were effectively characterized by the stress intensity factor. Residual stress was excluded from the calculation, suggesting that its impact on fatigue behaviour was negligible.

The fatigue propagation life of specimens with various defect types was analysed using a fracture mechanics approach. The initial crack dimensions and correction factors for calculating stress intensity factors were consistent with those applied in previous calculations. The analysis employed a modified "Paris" power law, as recommended by the JSSC guidelines, with the following formula and coefficients:

$$da/dN = C(\Delta K^n - \Delta K_{th}) \quad (3)$$

$$da/dN = 0, \; if \; \Delta K < \Delta K_{th} \quad (4)$$

The constants used in Eq. (3) the modified "Paris" power law were $C=1.5\times10^{-11}$ and n = 2.75, based on the mean curve values recommended by JSSC19. Additionally, the threshold value for the stress intensity factor range was specified in Eq. (4) as $\Delta K_{th}=2.9$ (units in MPa$\sqrt{m}$).

To evaluate the influence of stress distribution on crack propagation, an analysis was performed both with and without incorporating the correction factor F_g. Residual stress was excluded from this calculation. The results of the analysis were compared with fatigue testing outcomes. When the nominal stress was used without considering F_g, the crack propagation analysis showed highly conservative results for specimens containing CR and IP type defects compared to LOF, SI, and BH defects. Conversely, including the effect of stress distribution through F_g produced results consistent across defect types, aligning closely with findings from fatigue testing. This indicated that differences among defect types, as observed in S-N diagrams, were primarily influenced by stress distribution near the defects.

These findings highlighted the importance of considering stress distribution relative to weld bead configuration in crack propagation analysis by incorporating F_g. The residual stress, however, appears to have negligible effects on the analysis results. Additionally, the analysis revealed that crack propagation predictions tend to be conservative in the long fatigue life region, likely due to the inclusion of fatigue initiation life, as identified through beach-marking tests. However, in the low-cycle fatigue life region, the crack propagation analysis did not yield conservative results.

5. Product standards

Common standards for steel include ASTM (e.g., ASTM A36 for carbon structural steel), EN (e.g., EN 10025 for structural steels), and JIS (e.g., JIS G3101 for general structural steel). For welds, applicable standards include AWS (e.g., AWS D1.1 for structural welding), ISO (e.g., ISO 9606 for welder qualification), and BS (e.g., BS EN 13479 for welding consumables). These standards ensured consistency and clarity in material specifications and welding processes.

6. Future research directions

Future research directions in welding flaws and defects characteristics could focus on several key areas to improve understanding and mitigation of defects in welded structures. First, further investigation into the precise mechanisms of weld defect formation, including the influence of welding parameters and material properties, was essential for developing more effective defect detection methods. Additionally, research could explore advanced non-destructive testing (NDT) techniques, such as ultrasonics, X-ray, and digital imaging, for more accurate and efficient detection of internal weld flaws. The impact of welding flaws on the long-term fatigue performance and structural integrity of welded joints also warrants deeper exploration, especially under complex loading conditions. Furthermore, research into the development of new welding materials and techniques, such as friction stir welding or additive manufacturing, may offer insights into reducing flaw formation and improving the overall quality of welded joints. Finally, investigations into the role of residual stresses and their interaction with weld flaws in the context of crack propagation could lead to better predictive models for the service life of welded structures.

7. Conclusion

According to the discussion, the following could be concluded. This review highlighted significant strides in understanding the

mechanical properties, crack behavior, and fatigue performance of friction stir welds (FSWs) and flash butt welds (FBWs) for structural steel construction application. Both welding techniques are widely used in various applications due to their advantages in joint integrity and overall strength.

1. Friction Stir Welding (FSW) is known for producing high-quality, defect-free welds with minimal distortion, and it significantly reduces the likelihood of crack formation, especially in the heat-affected zone (HAZ). It is particularly advantageous in materials susceptible to cracking, as the process operates at lower temperatures compared to traditional welding methods. The fine-grained microstructure produced by FSW enhances fatigue resistance, making it an excellent choice for applications requiring durability under cyclic loading. FSW also results in a homogeneous microstructure with less porosity, which contributes to improved fatigue strength.
2. On the other hand, Flash Butt Welding (FBW) is highly efficient and effective for joining large sections of steel, especially in rail construction. However, FBW often results in a more heterogeneous microstructure and can lead to significant variations in the HAZ, which can increase the risk of crack formation, especially in the coarse-grained HAZ (CGHAZ). While FBW provides high joint strength and productivity, it may not offer the same fatigue resistance as FSW, particularly in areas with complex stress distributions. The HAZ in FBW typically shows a higher tendency for fatigue cracking due to the thermal gradients and rapid cooling rates involved.
3. Despite FSW's prominence in joining diverse materials for industries like aerospace and automotive, challenges remain regarding heat-induced precipitate weakening and defect formation in dissimilar welds. Similarly, FBW excels in rail joining, where improvements in temperature distribution, joint strength, and process parameters enhance fatigue resistance and weld quality.
4. Continued investigation into the microstructural evolution, particularly within the heat-affected zone (HAZ), and the development of innovative weld evaluation techniques were crucial for optimizing welding processes to meet the rigorous demands of modern engineering applications. The HAZ in FBW is more susceptible to variations, including coarse grain formation, which can reduce mechanical properties. FSW produces a more uniform HAZ, leading to better overall weld integrity.
5. FSW typically performs better than FBW in terms of crack resistance due to its lower processing temperatures and finer microstructure, which reduce the risk of cracking in the HAZ.
6. FSW offers superior fatigue resistance compared to FBW. The refined microstructure and minimized defects in FSW lead to better performance under cyclic loading conditions.

Friction Stir Welding is generally considered the superior technique when comparing crack resistance, HAZ integrity, and fatigue resistance, especially in applications requiring high durability. While Flash Butt Welding offers advantages in terms of speed and efficiency, particularly in large-scale structural steel constructions, it may not match FSW in terms of long-term performance and structural integrity. Therefore, for applications where crack resistance, fatigue strength, and optimal HAZ are critical, FSW is recommended over FBW.

14. Disclosure Statement

The authors declare that there were no conflicts of interest regarding the

publication of this article. The research was conducted independently, and no funding bodies influenced the study design, data collection, analysis, interpretation, or the decision to submit the article for publication. All authors have approved the final manuscript and confirm that it has not been previously published or submitted for consideration elsewhere.

REFERENCES

Alemdar A. S. A., Jalal S. R., Mulapeer M. M. (2023), *Effect of exfoliation corrosion on the efficient hybrid joint of AA2024-T3 and AA2198-T8 formed by friction stir welding*, Heliyon 9(6): e16577, DOI:10.1016/j.heliyon.2023.e16577

Aune S., Morin D., Langseth M., Clausen A. H. (2024), *Experimental and numerical study on the tensile ductility of an aluminium alloy with heat-affected zones*, European Journal of Mechanics-A/ Solids 105: 105239, DOI:10.1016/ j.euromechsol. 2024.105239

Baek S., Kim J., Kwak T., Lee T., Lee H. C., Chen C., Kim D. (2024), *Al heat affected zone-less resistance element welded lap joints of Al alloy and 1 GPa class steel: Transition of microstructure and fracture with heat transfer*, Journal of Materials Research and Technology 28: 3541-3565, DOI:10.1016/ j.jmrt.2023.12. 210

Bai W., Xu X., Liu Y., Liang Y., Shen Y., Han Z., Zhu M. (2023), *Microstructural evolutions and impact toughness in simulated welding heat affected zones for a high-strength carbide-free bainitic rail steel,* Materials Science and Engineering: A 880: 145325, DOI:10.1016/ j.msea.2023.145325

Bauri L. F., Alves L. H. D., Pereira H. B., Tschiptschin A. P., Goldenstein H. (2020), *The role of welding parameters on the control of the microstructure and mechanical properties of rails welded using FBW*, Journal of Materials Research and Tech. 9(4): 8058-8073, DOI:10.1016/j.jmrt. 2020.05.030

Celotto A., Sandnes L., Grong Ø., Sørhaug J. A., Stefani G., Wan D., Berto F. (2024), *Cold butt welding of dissimilar aluminum alloys: Characterization and interface bonding conditions*, Materials Science and Engineering: A 897: 146279, DOI:10.1016/ j.msea.2024.146279

Chen Y., Su S., Li Q., Yang H. (2019), *Multi-sensor data fusion for online quality assurance in flash welding,* Procedia Manufacturing, 34: 857-866, DOI:10.1016/j.promfg.2019.06.162

Cui C., Liu W. B., Tian Y. X., Zhang Q. H. (2024), *Fatigue experiment and assessment of Q420qFNH weathering steel in the unequal-thickness butt-welded joint,* Journal of Constructional Steel Research 220: 108839, DOI:10.1016/j.jcsr.2024. 108839

El-Sayed M. M., Shash A. Y., Abd-Rabou M., El-Sherbiny M. G. (2021), *Welding and processing of metallic materials by using friction stir technique: A review,* Journal of Advanced Joining Processes 3: 100059. DOI:10.1016/ j.jajp.2021.100059

Ghazanfari M., Tehrani P. H. (2021), *Increasing fatigue crack initiation life in butt-welded UIC60 rail by optimization of welding process parameters*, International Journal of Fatigue 151: 106367, DOI:10.1016/ j.ijfatigue.2021.106367

Hu J., Zhang Q., Yang Q., Xu X., Xu C., Lv J., Hu Y. (2023), *Cause analysis of surface cracks in flash butt welding joint of high manganese steel frog*, Engineering Failure Analysis 154: 107683, DOI:10.1016/ j.engfailanal.2023.107683

Isa M. S. M., Moghadasi K., Ariffin M. A., Raja S., bin Muhamad M. R., Yusof F., bin Ab Karim M. S. (2021), *Recent research progress in friction stir welding of aluminium and copper dissimilar joint: a review*, Journal of Materials Research and Technology 15: 2735-2780, DOI:10.1016/j.jmrt. 2021.09.037

Godefroid L. B., Faria G. L. D., Cândido L. C., Viana T. G. (2014), *Fatigue failure of a flash butt welded rail*, Procedia Materials Science 3: 1896-1901, DOI:10.1016/j.mspro.2014.06.306

Kermanidis A. T., Tzamtzis A. (2017), *An experimental approach for estimating the effect of heat affected zone (HAZ) microstructural gradient on fatigue crack growth rate in aluminum alloy FSW*, Materials Science and Engineering: A 691: 110-120, DOI:10.1016/j.msea.2017.03.036

Khaliq U. A., Muhamad M. R., Yusof F., Ibrahim S., Isa M. S. M., Chen Z., Çam G. (2023), *A review on friction stir butt welding of aluminum with magnesium: A new insight on joining mechanisms by interfacial enhancement*, Journal of Materials Research and Technology 27: 4595-4624 DOI:10.1016/ j.jmrt.2023.10.158

Królicka A., Radwański K., Kuziak R., Zygmunt T., Ambroziak A. (2020), *Microstructure-based approach to the evaluation of welded joints of bainitic rails designed for high-speed railways,* Journal of Constructional Steel

Research 175: 106372, DOI:10.1016/j.jcsr.2020.106372

Lepore M., Berto F. (2019), *On the fatigue propagation of multiple cracks in friction stir weldments using linear and non-linear models under cyclic tensile loading*, Engineering Fracture Mechanics 206: 463-484, DOI:10.1016/j.engfracmech.2018.12.015

Li M., Xu P., Zhou L., Wei Z., Liang Y. (2020), *Better mechanical properties via uniform microstructure architecture in flash-butt welded TA19 joints*, Materials Science and Engineering: A 788: 139545, DOI:10.1016/j.msea.2020.139545

Li X., Ma R., Liu X., Lv Q., Wang X., Tian Z. (2022), *Effect of laser shock peening on fatigue properties of U75VG rail flash-butt welding joints*, Optics and Laser Technology 149: 107889, DOI:10.1016/j.optlastec.2022.107889

Liu J., Li J., Li X., Jin F., Du Y., Shi J., Xiong J. (2023), *Fatigue fracture behavior of a Ti17 joint under various heat treatment specifications prepared by linear friction welding*, Materials Characterization 205: 113318, DOI:10.1016/j.matchar.2023.113318

Liu T., Gao S., Ye W., Shi L., Kumar S., Qiao J. (2023), *Achievement of high-quality joints and regulation of intermetallic compounds in ultrasonic vibration enhanced friction stir lap welding of aluminum/steel*, Journal of Materials Research and Technology 25: 5096-5109, DOI:10.1016/j.jmrt. 2023.06.251

Maia P. P., Miná É. M., Dalpiaz G., Marinho R. R., Paes M. T., Motta M. F., Silva C. C. (2023), *Microstructural characterisation and micromechanical investigation of the heat-affected zone in multi-pass welding of 9Ni steel pipes*, Journal of Materials Research and Technology 24: 1716-1732, DOI:10.1016/j.jmrt.2023.03.092

Miao H., Tsutsumi S., Yamashita T., Morisada Y., Fujii H. (2023), *Fatigue strength improvement of linear friction welded butt joints of low carbon steel by pressurizing after oscillation*, Journal of Manufacturing Processes 102: 795-805, DOI:10. 1016/j.jmapro.2023.08.004

Miao H., Yamashita T., Tsutsumi S., Morisada Y., Fujii H. (2024), *Multiple analyses of factors influencing fatigue life of linear friction welded low carbon steel,* Journal of Adv. Joining Processes 9: 100201, DOI:10.1016/j.jajp.2024.100201

Miki C., Fahimuddin F., Anami K. (2001), *Fatigue performance of butt-welded joints containing various embedded defects*, Doboku Gakkai Ronbunshu 668: 29-41, DOI:10.2208/jscej.2001. 668_29

Mishra A., Gangil N., Siddiquee A. N., Khan Y. S., Bhardwaj T., Singh D. K. (2023), *Microstructural investigation on linear friction welded stainless steel and medium carbon steel,* Materials Today: Proceedings, DOI:10. 1016/j.matpr.2023.04.672

Ogunsemi B. T., Abioye T. E., Ogedengbe T. I., Zuhailawati H. (2021), *A review of various improvement strategies for joint quality of AA 6061-T6 friction stir weldments,* Journal of Materials Research and Technology 11: 1061-1089, DOI:10.1016/j.jmrt.2021.01.070

Owsiński R., Lachowicz D. S., Lachowicz C. T., Gil R., Niesłony A. (2021), *Characterisation of joint properties through spatial mapping of cracks in fatigue specimens, extracted from the linearly friction welded steel coupon*, Precision Engineering 71: 78-89, DOI:10.1016/j.precisioneng.2021.02.008

Pang Y., Grilli N., Su H., Liu W., Ma J., Yu S. F. (2022), *Experimental investigation on microstructures and mechanical properties of PG4 flash-butt rail welds*, Engineering Failure Analysis 141: 106650, DOI:10.1016/j.engfailanal. 2022.106650

Patel V., Wouters H., Baghdadchi A., De Backer J., Igestrand M., Azimi S., Andersson J. (2023), *Robotic friction stir welding in lightweight battery assembly of extrusion-cast aluminium alloys*, Journal of Advanced Joining Processes 8: 100156, DOI:10.1016/j.jajp.2023.100156

Peng H., Wu Y. X., Zhang T., Chen S. Y., Zhang C. (2024), *Residual stresses in linear friction welding of TC17 titanium alloy considering phase fraction*, Trans. of Nonferrous Metals Soc. of China 34(1): 184-193, DOI:10.1016/S1003-6326 (23)66390-3

Peng M., Liu H., Xuan Y., Liu X., Xu L., Yu Z. (2021), *Evaluation of the microstructural and mechanical properties of ductile cast iron and alloy steel dissimilar materials welded by magnetically impelled arc butt,* Journal of Materials Research and Technology 15: 4623-4635, DOI:10.1016/j.jmrt. 2021.10.059

Pereira H. B., Echeverri E. A. A., Alves L. H. D., Yildirimli K., Lewis R., Goldenstein H. (2024), *Influence of HAZ microstructure on RCF under twin-disc test of a flash-butt welded rail*, Wear 546: 205324, DOI:10.1016/j.wear.2024. 205324

Porcaro R. R., Faria G. L., Godefroid L. B., Apolonio G. R., Cândido L. C., Pinto E. S. (2019), *Microstructure and mechanical properties of a flash butt welded pearlitic*

rail, Journal of Materials Processing Technology 270: 20-27, DOI:10.1016/j.jmatprotec.2019.02.013

Prabhakar D. A. P., Shettigar A. K., Herbert M. A., Pimenov D. Y., Giasin K., Prakash C. (2022), *A comprehensive review of friction stir techniques in structural materials and alloys: challenges and trends*, Journal of Materials Research and Technology 20: 3025-3060, DOI:10.1016/j.jmrt. 2022.08.034

Puspitasari P. (2024), *Fatigue crack growth rate and mechanical properties of one-step double-side friction stir welded AA6061-T6,* Results in Engineering 21: 101958, DOI:10.1016/j.rineng.2024.101958

Rajesh K. R., Devaraj S. (2021), *Selection of parameters for flash butt welding on mild steel brake tension rods,* Materials Today: Proceedings 45: 191-196, DOI:10.1016/j.matpr.2020.10.416

Shajan N., Arora K. S., Shome M. (2019), *Correlation between grain misorientation, texture and impact toughness across a flash butt weld of HSLA steel*, Materials Letters 236: 436-439, DOI:10.1016/j.matlet.2018.10.153

Shen J., Wei Z., Zhu X., Liang Y., Liang Y., Jiang F., Xiao Z. (2018), *Microstructure evolution and mechanical properties of flash butt-welded Inconel718 joints*, Materials Science and Engineering: A 718: 34-42, DOI:10.1016/j.msea. 2018.01.104

Shen M., Mei L., Gong F., Li C., Li Q. (2024), *Damage Behaviour of Rail Flash-butt Welding Joints under Controlled Impact Kinetic Energy,* Wear 552: 205435, DOI:10.1016/j.wear.2024. 205435

Sheng X., Lin C., Zheng W., Zhu Z., Song X. (2024), *Study on fatigue life of high-strength steel rebars joined by flash butt welding based on experimental and machine learning approaches*, Engineering Failure Analysis 156: 107812, DOI:10.1016/j.engfailanal.2023.107812

Sheng X. W., Zheng W. Q., Yang Y. (2020), *Tensile and high-cycle fatigue performance of HRB500 high-strength steel rebars joined by flash butt welding*, Const. and Building Materials 241: 118037, DOI:10.1016/j.conbuildmat.2020.118037

Silva Y. C. D., Andrade T. C., Júnior F. O., Sousa A. B. F., dos Santos J. F., Marcondes F., Silva C. C. (2023), *Numerical investigation of the influence of friction stir welding parameters on the microstructure of AISI 410S ferritic stainless steel joints,* Journal of Materials Research and Technology 27: 8344-8359, DOI:10.1016/j.jmrt. 2023.11.054

Singh K., Singh G., Singh H. (2018), *Review on friction stir welding of magnesium alloys,* Journal of Magnesium and Alloys 6(4): 399-416, DOI:10. 1016/j.jma.2018.06.001

Śliwa R. E., Myśliwiec P., Ostrowski R., Bujny M. (2019), *Possibilities of joining different metallic parts of structure using friction stir welding methods,* Procedia Manufacturing 27: 158-165, DOI: 10.1016/j.promfg.2018.12.059

Su H., Pun C. L., Mutton P., Kan Q., Kang G., Yan W. (2021), *Numerical study on the ratcheting performance of rail flash butt welds in heavy haul operations,* International Journal of Mechanical Sciences 199: 106434, DOI:10.1016/ j.ijmecsci.2021. 106434

Su H., Li J., Lai Q., Pun C. L., Mutton P., Kan Q., Yan W. (2020), *Ratcheting behaviour of flash butt welds in heat-treated hypereutectoid steel rails under uniaxial and biaxial cyclic loadings,* International Journal of Mechanical Sciences 176: 105539, DOI:10.1016/j.ijmecsci.2020. 105539

Tiejun M. A., Zhenguo G., Xiawei Y., Junlong J., Xi C., Jun T., Liukuan Y. (2024), *Plastic flow and interfacial bonding behaviors of embedded linear friction welding process: Numerical simulation combined with thermo-physical experiment,* Chinese Journal of Aeronautics, DOI:10.1016/j.cja.2023.12.034

Trimech M., Annan C. D., Walbridge S., Maljaars J. (2023), *Fatigue behaviour of butt-lap friction stir welded joints used with aluminum bridge decks,* Structures 51: 1795-1805, DOI:10.1016/j.istruc. 2023.03.151

Vieltorf F., Wolfrum M., Zens A., Wenzler D. L., Sigl M. E., Zaeh M. F. (2024), *Effects of alignment discrepancies on the weld quality in friction stir welding*, Journal of Advanced Joining Processes 9: 100190, DOI:10.1016/j.jajp.2024. 100190

Wang F. F., Li W. Y., Shen J., Hu S. Y., Dos Santos J. F. (2015), *Effect of tool rotational speed on the microstructure and mechanical properties of bobbin tool friction stir welding of Al–Li alloy,* Materials and Design 86: 933-940, DOI:10.1016/j.matdes. 2015.07.096

Wang J., Ma C., Han J., Jiang Z., Linton V. (2021), *Acquisition of HSLA steel weld joints with excellent mechanical performance through flash butt welding physical simulation,* Materials Letters 303: 130511, DOI:10.1016/j.matlet.2021.130511

Wu Y., Pun C. L., Su H., Huang P., Welsby D., Mutton P., Yan W. (2022), *Numerical study on ratcheting performance of heavy haul rail flash-butt welds in curved tracks*, Engineering Failure Analysis 140: 106611, DOI:10.1016/j.engfailanal. 2022.106611

Xiao X., Cheng D., Li H., Zhang C., Zhang F., Qi A. (2024), *Microstructure analysis of 7050 aluminum alloy joint fabricated by linear friction weld*, International Journal of Lightweight Materials and Manufacture 7(4): 520-530. DOI:10 .1016/ j.ijlmm.2024.03.008

Xi C., Sun D., Xuan Z., Wang J., Song G. (2016), *Microstructures and mechanical properties of flash butt welded high strength steel joints,* Materials and Design 96: 506-514, DOI:10.1016/j.matdes.2016. 01.129

Xu N., Qiu Z. H., Ren Z. K., Shen J., Wang D., Song Q. N., Bao Y. F. (2023), *Enhanced strength and ductility of rapid cooling friction stir welded ultralight Mg–14Li–1Al alloy joint*, Journal of Materials Research and Technology 23: 4444-4453, DOI:10.1016/ j.jmrt.2023.02.083

Xu P., Zhou L., Han M., Wei Z., Liang Y. (2020), *Flash-butt welded Ti6242 joints preserved base-material strength and ductility*, Materials Science and Engineering: A 774: 138915, DOI:10.1016/ j.msea.2020.138915

Xu R., Zhang M., Gao Z., Zhao G., Ding W., Wang S., Li J. (2024), *Temperature field calculation of rail flash welding,* High-speed Railway 2(2): 116-121, DOI: 10.1016/j.hspr.2024.03.001

Xu Y., Yang B., Shi Y., Feng X., Li J., Feng C., Volodymyr K. (2022), *Quality reliability analysis of flash welding joint of cold-rolled 50JW800 silicon steel strip,* Engineering Failure Analysis 138: 106292, DOI:10.1016/ j.engfailanal.2022.106292

Xu Z., Lu P., Shu Y. (2016), *Microstructure and fracture mechanism of a flash butt welded 380CL steel*, Engineering Failure Analysis 62: 199-207, DOI:10.1016/j.engfailanal.2016.02.005

Yan R., Mela K., Yang F., El Bamby H., Veljkovic M. (2023), *Equivalent material properties of the heat-affected zone in welded cold-formed rectangular hollow section connections*, Thin-Walled Structures 184: 110479, DOI:10.1016/ j.tws.2022. 110479

Yan R., Xin H., Yang F., El Bamby H., Veljkovic M., Mela, K. (2022), *A method for determining the constitutive model of the heat-affected zone using digital image correlation*, Construction and Building Materials 342: 127981, DOI:10.1016/ j.conbuildmat.2022.127981

Yang X., Ma S., Chu Q., Peng C., Su Y., Xiao B., Li W. (2023), *Investigation of microstructure and mechanical properties of GH4169 superalloy joint produced by linear friction welding*, Journal of Materials Research and Technology 24: 8373-8390, DOI:10.1016/ j.jmrt.2023.05.081

Yang X., Meng T., Su Y., He X., Guo Z., Wu D., Li W. (2024), *The effect of inclusions and pores on creep crack propagation of linear friction welded joints of GH4169 superalloy,* Journal of Materials Research and Technology 29: 4636-4649, DOI:10.1016/ j.jmrt. 2024.02.154

Yasui T., Wu-Bian T., Hanai A., Mori T., Hirosawa K., Fukumoto M. (2018), *Friction stir girth welding between aluminum and steel rods*, Procedia Manufacturing 15: 1376-1381, DOI:10.1016/ j.promfg.2018.07.345

Yu S., Xiawei Y., Tingxi M., Dong W., Rui X. U., Haiyu X., Shuo Y. (2024), *Effect of linear friction welding process on microstructure evolution, mechanical properties, and corrosion behavior of GH4169 superalloy,* Chinese J. of Aeronautics 37(6): 504-520, DOI:10.1016/j.cja.2024.03.039

Yu S., Xiawei Y, Tingxi M., Xinyuan H., Dong W., Wenya L., Shuo Y. (2024), *Strengthening mechanism and forming control of linear friction welded GH4169 alloy joints,* Chinese Journal of Aeronautics 37(4): 609-626, DOI:10.1016/j.cja. 2024.01.026

Yu X., Feng L., Qin S., Zhang Y., He Y. (2015), *Fracture analysis of U71Mn rail flash-butt welding joint*, Case Studies in Engineering Failure Analysis 4: 20-25, DOI:10.1016/ j.csefa.2015.05.001

Zhang T., Ji H., Xu D., Yin X., Wei H., Sun Z., Liu C. (2023), *A hybrid shoulder to achieve a significant improvement in tensile strength and fatigue performance of friction stir welded joints for Al–Mg–Si alloy*, Journal of Materials Research and Technology 27: 2280-2291, DOI:10.1016/ j.jmrt. 2023.10.067

Zhang X., Zhang J., Yao Y., Qiao Q., Zhao L., Liu L., Li H. (2024), *Anomalous enhancing effects of electric pulse treatment on strength and ductility of TC17 linear friction welding joints,* Journal of Materials Science and Technology 203: 155-166, DOI:10. 1016/j.jmst.2024.04.008

Zhao X., Fan Y., Liu Y., Wang H., Dong P. (2015), *Evaluation of fatigue fracture mechanism in a flash butt welding joint of a U75V type steel for railroad applications*, Engineering Failure Analysis 55: 26-38, DOI: 10.1016/j.engfailanal. 2015.05.001

Zhou L., Lin T., Xu P., Liang Y., Liang Y. (2023), *Heterogeneous microstructure improves the strength and ductility of a flash-butt welded IN718 alloy joint*, Materials Science and Engineering: A 879: 145307, DOI:10.1016/j.msea.2023.145307

Zhou L., Xu P., Lin T., Zhu X., Liang Y., Liang Y. (2022), *Outstanding ductility of flash-butt welded Inconel 718 joints after post-weld heat treatment,* Materials Science and Engineering: A 843: 143132, DOI:10.1016/j.msea.2022.143132

Zhu X., Xu P., Liang Y., Wei Z., Liang Y. (2018), *Flash butt weldability of Inconel718 alloy,* Journal of Materials Processing Technology 258: 326-333, DOI: 10.1016/j.jmatprotec.2018.04.011

Received: 11 November 2024 • Revised: 26 December 2024 • Accepted: 9 January 2025